

1. Lipkin-Meshkov Glick model analysis

September 10, 2021

Jan Střeleček

The aim of this text is to analyze Hamiltonian

$$\hat{H} = \hat{J}_3 + \lambda \hat{V}_1 + \chi \hat{V}_2 + \chi^2 \hat{V}_3, \quad (1.1)$$

where

$$\hat{V}_1 = -\frac{1}{2j} \hat{J}_1^2 \quad (1.2)$$

$$\hat{V}_2 = -\frac{1}{2j} [\hat{J}_1(\hat{J}_3 + j\mathbb{1}) + (\hat{J}_3 + j\mathbb{1})\hat{J}_1] \quad (1.3)$$

$$\hat{V}_3 = -\frac{1}{2j} (\hat{J}_3 + j\mathbb{1})^2. \quad (1.4)$$

Using the Spherical harmonics basis $\{|j, m\rangle\}$ for quantum numbers j as the angular momentum and m its projection on the direction of \hat{J}_3 and defining

$$\hat{J}_{\pm} := \frac{1}{2}(\hat{J}_1 \pm i\hat{J}_2), \quad (1.5)$$

we get the matrix elements

$$\langle j'm' | \hat{J}^2 | jm \rangle = j(j+1)\delta_{j'j}\delta_{m'm} \quad (1.6)$$

$$\langle j'm' | \hat{J}_3 | jm \rangle = m\delta_{j'j}\delta_{m'm} \quad (1.7)$$

$$\langle j'm' | \hat{J}_{\pm} | jm \rangle = \sqrt{(j \mp m)(j \pm m + 1)}\delta_{j'j}\delta_{m'm\pm1}, \quad (1.8)$$

where $\delta_{a'b}$ is Kronecker delta. Hamiltonian in eq. 1.1 can then be written as

$$\begin{aligned} \hat{H} = & J_3 - \frac{\lambda}{8j}(J_+ + J_-)^2 - \frac{\chi}{4j} [(J_+ + J_-)(J_3 + j\mathbb{1}) + (J_3 + j\mathbb{1})(J_+ + J_-)] \\ & - \frac{\chi^2}{2j} (J_3 + j\mathbb{1})^2, \end{aligned} \quad (1.9)$$

which has pentadiagonal matrix representation. During the whole paper, $j = N/2$ will be used.

The behavior of dimensions $N = 1$ and $N = 2$ are fundamentally different from higher dimensions and, therefore, the discussion will start at $N = 3$, followed by $N = 5$. Then the limit $N \rightarrow \infty$ will be taken along with the generalization of some characteristics to an arbitrary dimension. Due to the complexity of our Hamiltonian, it is not possible to prove every statement analytically. Some numerical methods, supported by some basic theorems, are needed. All figures and simulations were calculated in Mathematica.

1.1 Case $N = 3$

The lowest dimension behaving similarly to higher N is 3 with the matrix represented Hamiltonian

$$\hat{H} = \begin{pmatrix} -\frac{\lambda+6}{4} & -\frac{\chi}{2\sqrt{3}} & -\frac{\lambda}{2\sqrt{3}} & 0 \\ -\frac{\chi}{2\sqrt{3}} & \frac{(-7\lambda-4\chi^2-6)}{12} & -\chi & -\frac{\lambda}{2\sqrt{3}} \\ -\frac{\lambda}{2\sqrt{3}} & -\chi & \frac{(-7\lambda-16\chi^2+6)}{12} & -\frac{5\chi}{2\sqrt{3}} \\ 0 & -\frac{\lambda}{2\sqrt{3}} & -\frac{5\chi}{2\sqrt{3}} & -\frac{\lambda}{4} - 3\chi^2 + \frac{3}{2} \end{pmatrix}. \quad (1.10)$$

The spectrum of this Hamiltonian can be calculated analytically using some substitutions G, F, D, E , see Appendix ??, as

$$E_0 = \frac{1}{12} \left(G - F - \frac{\sqrt{D - E}}{2} \right) \quad (1.11)$$

$$E_1 = \frac{1}{12} \left(G - F + \frac{\sqrt{D - E}}{2} \right) \quad (1.12)$$

$$E_2 = \frac{1}{12} \left(G + F - \frac{\sqrt{D + E}}{2} \right) \quad (1.13)$$

$$E_3 = \frac{1}{12} \left(G + F + \frac{\sqrt{D + E}}{2} \right). \quad (1.14)$$

Eigenvectors can also be written analytically, but doing it here would be redundant. On sections $\lambda = 1$ and $\chi = 1$, see Figures 1.1 resp. 1.2, it can be seen the general behaviour of the spectrum, where the energies get close to each other somewhere around the center of our coordinate system $(\lambda; \chi)$ and then separate monotonously to never meet again. In addition, the spectrum is symmetrical for $\chi \leftrightarrow -\chi$.

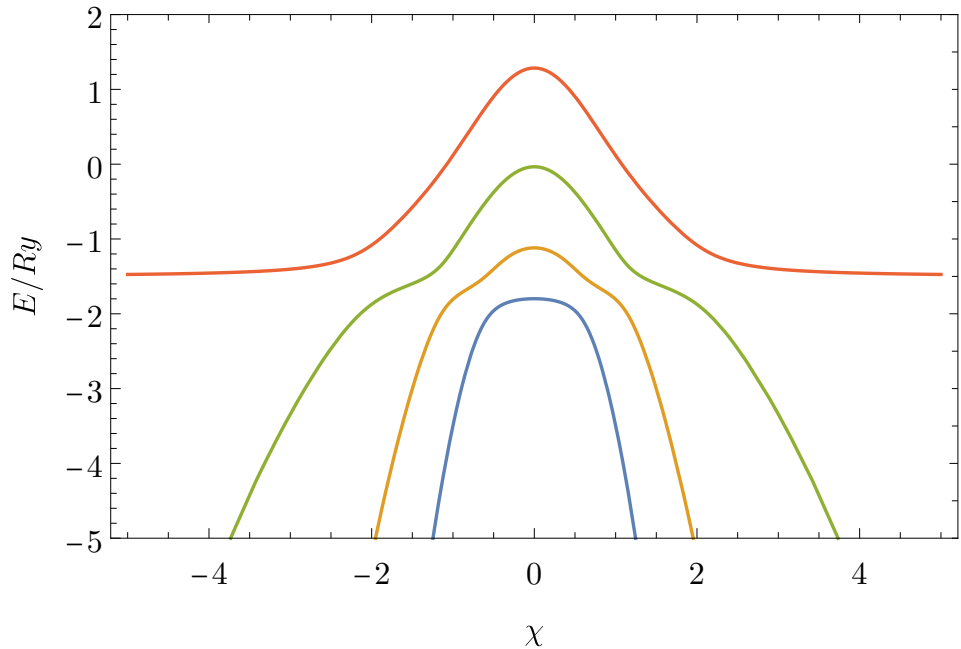


Figure 1.1: Energy for the case $N = 3$, section $\lambda = 1$

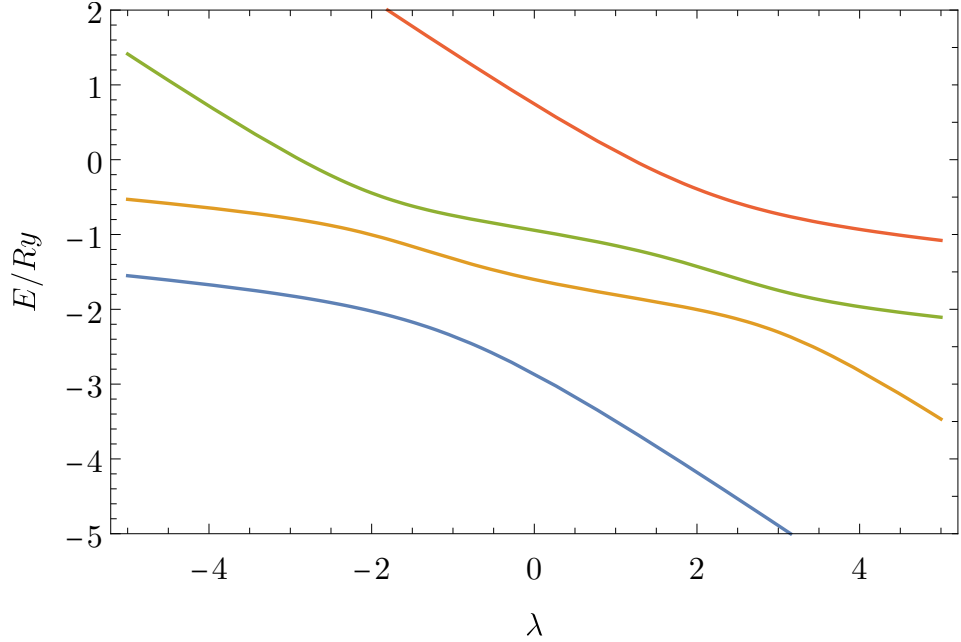


Figure 1.2: Energy for the case $N = 3$, section $\chi = 1$

From the Equations 1.11, 1.12 can be seen that there might exist degeneracy between every two neighboring energy levels¹. Specifically, for $E_0 = E_1$ for $D = E$, which for real values λ , χ has two solutions

$$(\lambda_d, \pm\chi_d) = \left(-\frac{1}{2}; \sqrt{\frac{3}{5}} \right).$$

Point-like characteristics correspond to Theorem ??, which states that Hamiltonian driven by two real parameters can be degenerated only on 0-dimensional manifolds.

If the energy spectrum is degenerate and the metric tensor diverges, see individual elements in Fig. 1.3, its determinant also diverges, as shown in Fig. 1.4, along with Christoffel symbols in Fig. 1.5. Note that the metric tensor determinant is positive definite, thus the manifold is Riemannian. Further on, it reflects the symmetry $\chi \leftrightarrow -\chi$, except for elements g_{12} , Γ_{121} , Γ_{211} , and Γ_{222} , which switch their sign.

¹If substituted letters were real numbers, degeneracies would exist between every two neighboring energy levels. The problem here, that for functions G, F, D, E the solution might not exist. Even though we will see that it's probably not that case and degeneracy exist between every two neighboring energy levels.

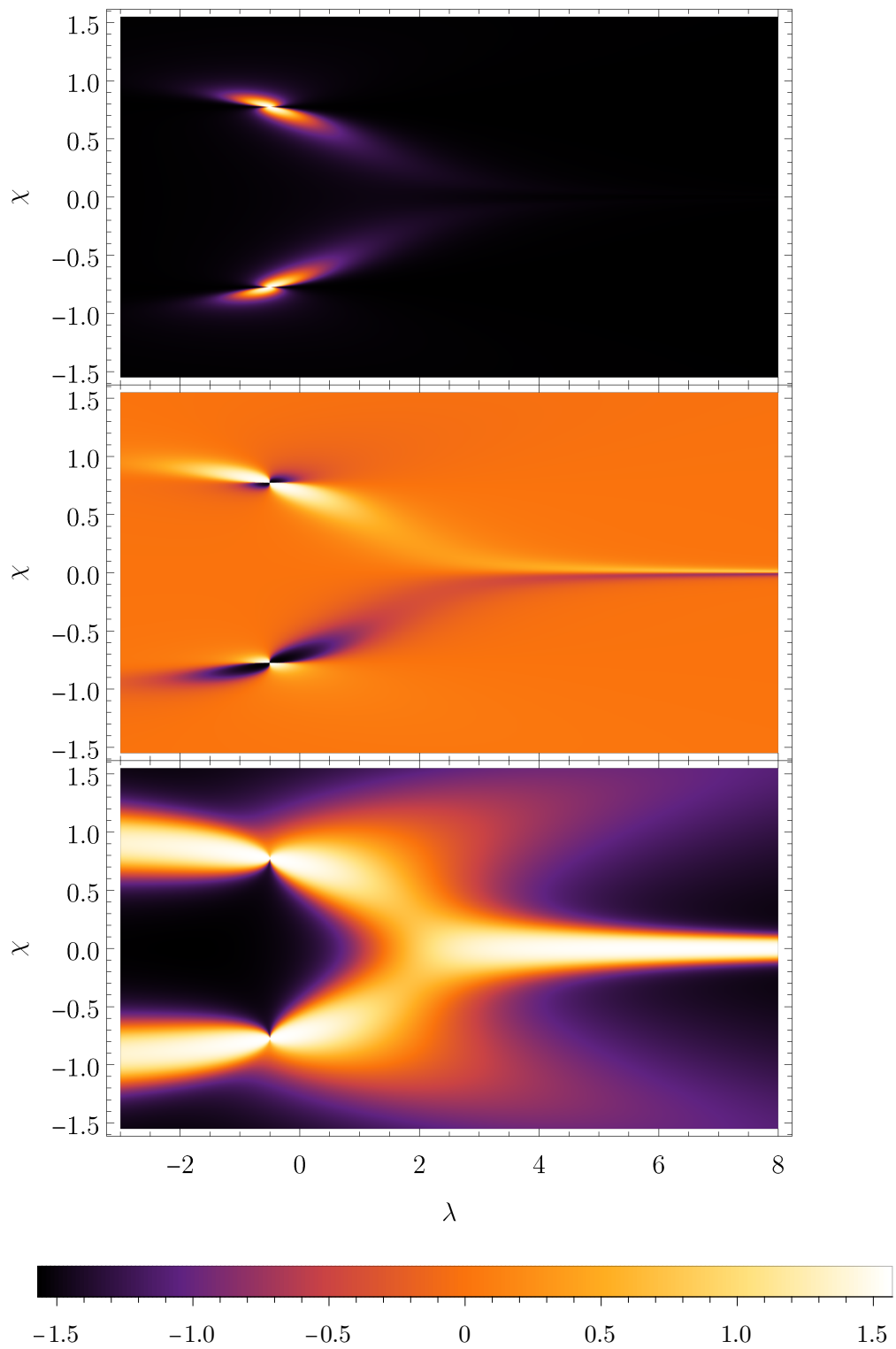


Figure 1.3: Arctangent of metric tensor elements for the case $N = 3$. From the top: $\text{Arctan}(g_{11})$, $\text{Arctan}(g_{12}) = \text{Arctan}(g_{21})$, $\text{Arctan}(g_{22})$

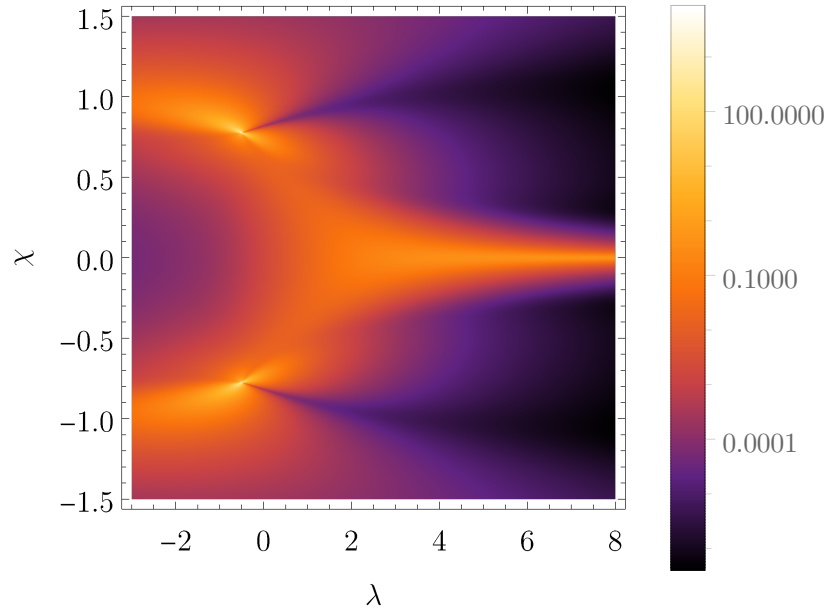


Figure 1.4: Metric tensor determinant in a parameter space for $N = 3$.

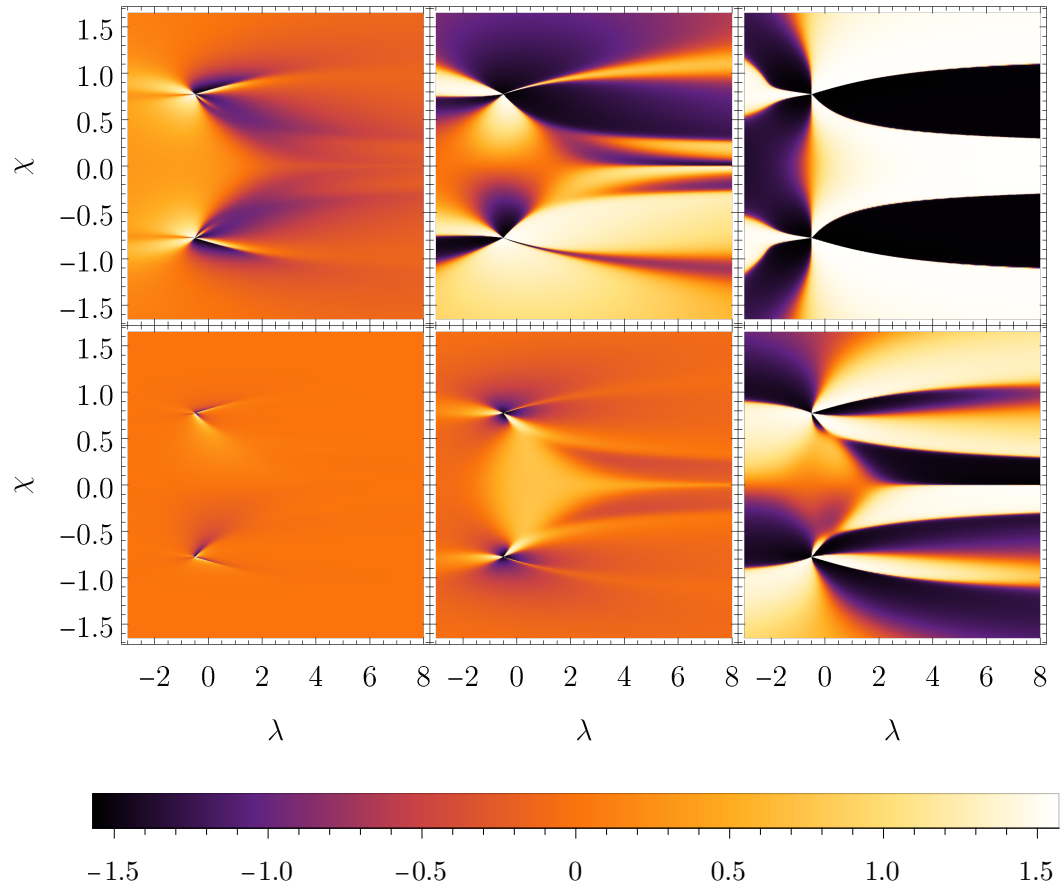


Figure 1.5: 1.0 Arctangent of Christoffel symbols for the case $N = 3$. First row from left: $\text{Arctan}(\Gamma_{111})$, $\text{Arctan}(\Gamma_{121})$, $\text{Arctan}(\Gamma_{122})$. Second row from left: $\text{Arctan}(\Gamma_{211})$, $\text{Arctan}(\Gamma_{221})$, $\text{Arctan}(\Gamma_{222})$.

Due to metric tensor degeneracy, the space is not geodesically maximal. To see that the singularity is not the only *coordinate one*², the Ricci scalar can be calculated, see Fig. 1.6. Divergent Ricci scalar implies the existence of a *physical singularity*. This can be seen from the sections in χ -direction drawn in Fig. 1.7, which at coordinate $(\lambda_d; \chi_d)$ diverges, implying the singularity is *physical*.

The presence of singularities means that our ground state manifold is geodesically incomplete and according to Theorem ?? there exist some geodesically unreachable coordinates.

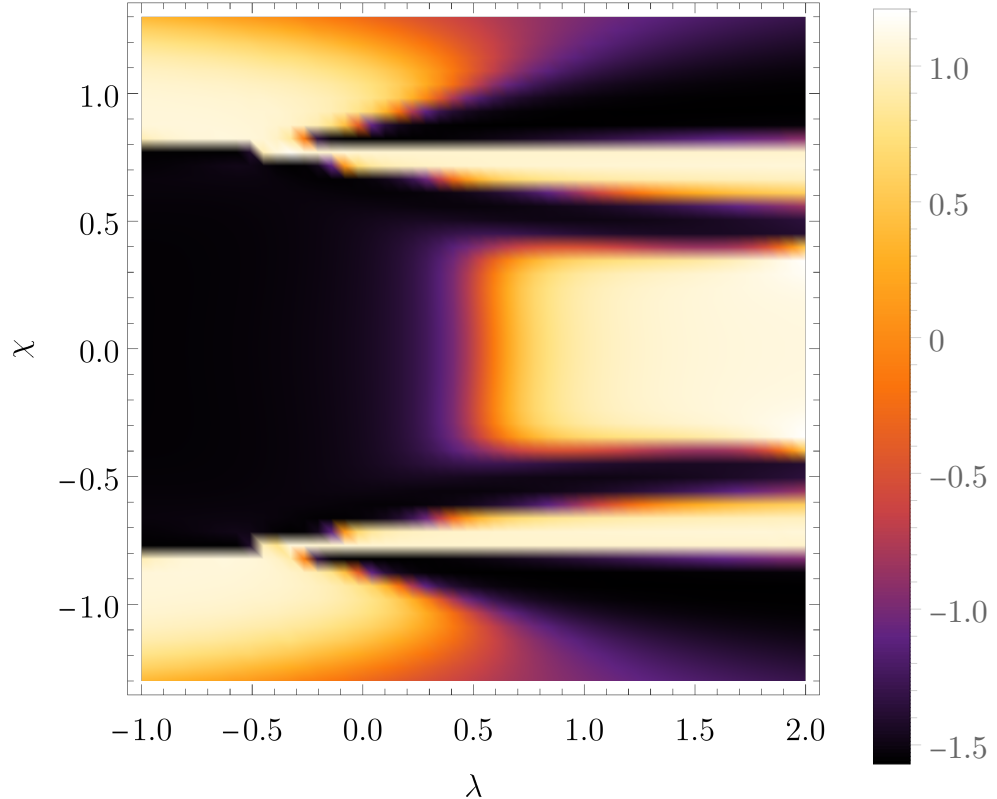


Figure 1.6: Arctangent of Ricci curvature for the case $N = 3$. [Excuse the resolution, I will make better calculation in Metacentrum later.](#)

²Coordinate singularity is present only in some coordinates. This is different from so called *physical singularity*, which is present in every choice of the coordinate system.

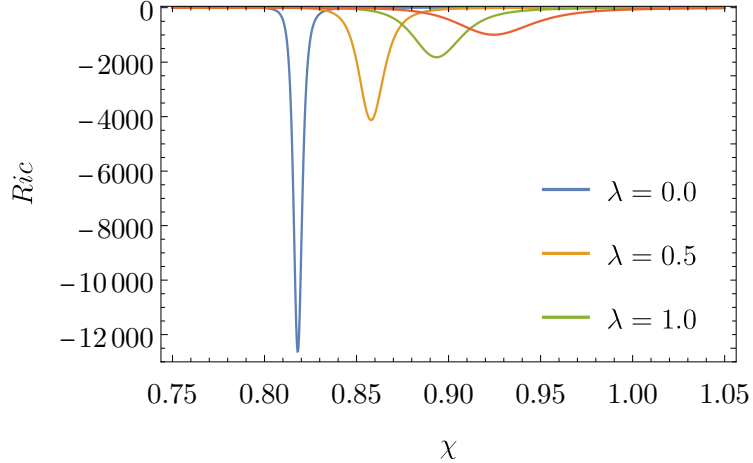


Figure 1.7: Ricci curvature sections for three different $\lambda = \text{const.}$

The system characteristics can be seen more clearly from geodesics, i.e., by solving the initial value problem with conditions

$$(\lambda(t_i); \chi(t_i)) = (\lambda_i; \chi_i)$$

$$\left. \left(\frac{d\lambda(t)}{dt}; \frac{d\chi(t)}{dt} \right) \right|_{t_i} = (\lambda'_i; \chi'_i),$$

where t_i means *initial time*.

Results for these geodesics starting at $(\lambda; \chi) = (0; 0)$, $(\lambda', \chi') = (\cos \theta; \sin \theta)$ for $\theta \in [-0.63; 0.63]$ and $\theta \in [\pi - 0.225; \pi + 0.225]$ with step $\Delta\theta = 0.01$, can be seen in Fig. 1.8. Other values θ result in a close approach of the geodesics to the singularity, making the calculations numerically unstable. The fact that geodesics lean towards singularities is well known from the theory of General Relativity (GR). The main difference here is that our "test particle" seems to be partially repulsed by the singularity. The analogy with GR would therefore fail because of the nonexistence of negative mass and gravitational dipoles. The better analogy would be electromagnetism, which has a downside in the fact that one does not usually use the metric structures in this theory. Comparison of those two intuitive examples can be seen in Fig. 1.9. The geodesic behavior is not caused only by the singularity but also by a large Ricci curvature leaning to the right from it. This means that the distance across this gap is also large, leading to the strong tendency of the geodesics to go around the singularity rather than crossing it, which is again seen in Fig. 1.8.

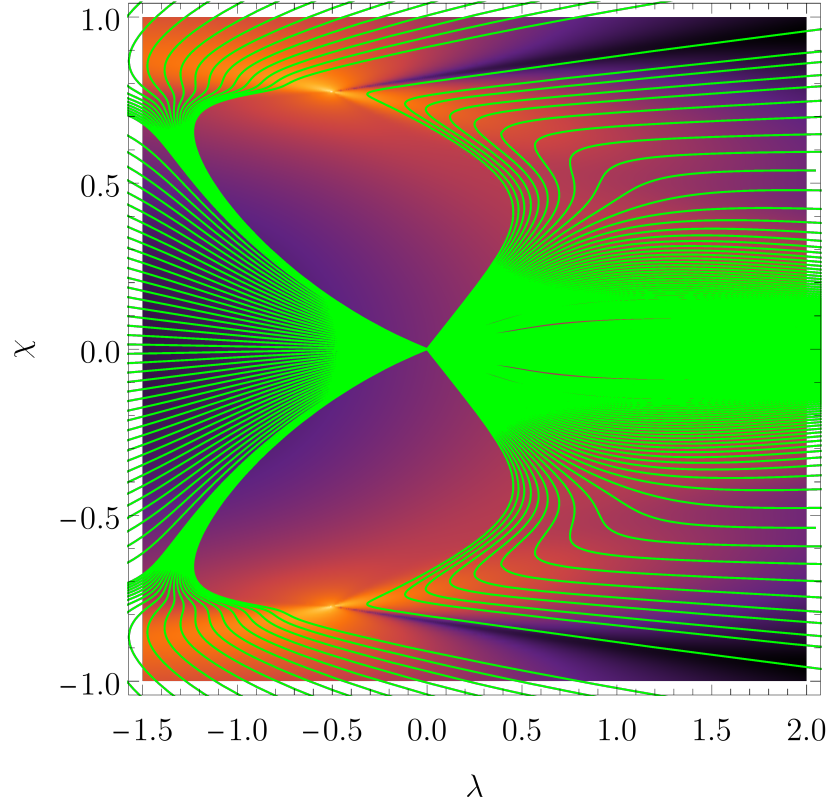


Figure 1.8: Geodesics for the case $N = 3$ starting from $(\lambda_i; \chi_i) = (0; 0)$ with $(\lambda'_i; \chi'_i) = (\cos \theta; \sin \theta)$, parametrized by angle θ .

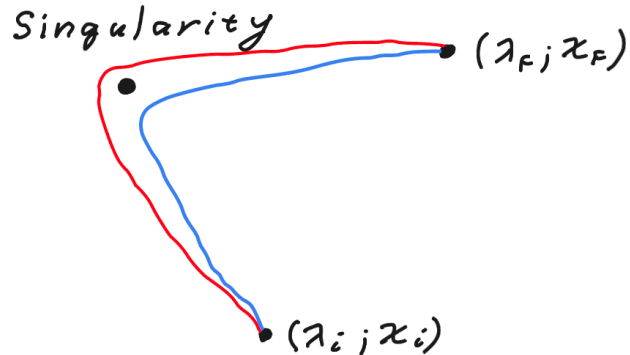


Figure 1.9: Comparing geodesics with repulsing (blue) and attracting (red) metric tensor divergence in the spherical symmetrical space.

1.2 Case $N = 5$

Few characteristics in arbitrary dimension can be shown for the case $N = 5$. First are the degeneracies between different energy levels, which can be seen in Fig. 1.10. One can see that only $E_0 = E_1$ the degeneracy lies on the separatrix and all others are distributed around. The $\chi \leftrightarrow -\chi$ symmetry holds for all of them.

Another fact, which is good to realize, is how the space itself looks like. This is best seen from the metric tensor determinant, fig. 1.11.

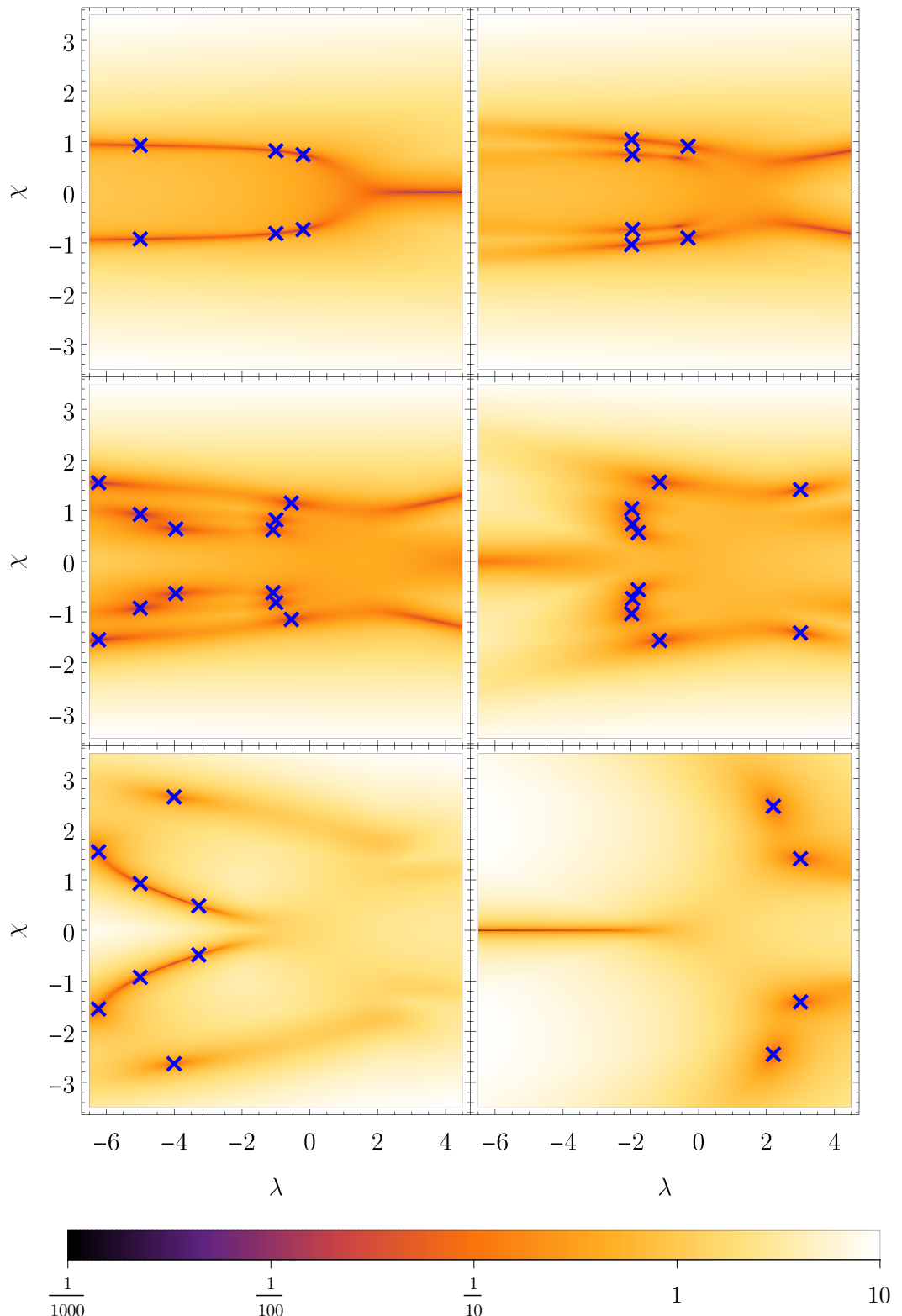


Figure 1.10: Energy differences between neighboring energy levels for $N = 5$. First row: $E_1 - E_0$, $E_2 - E_1$, second row: $E_3 - E_2$, $E_4 - E_3$, third row: $E_5 - E_4$, $E_6 - E_5$.

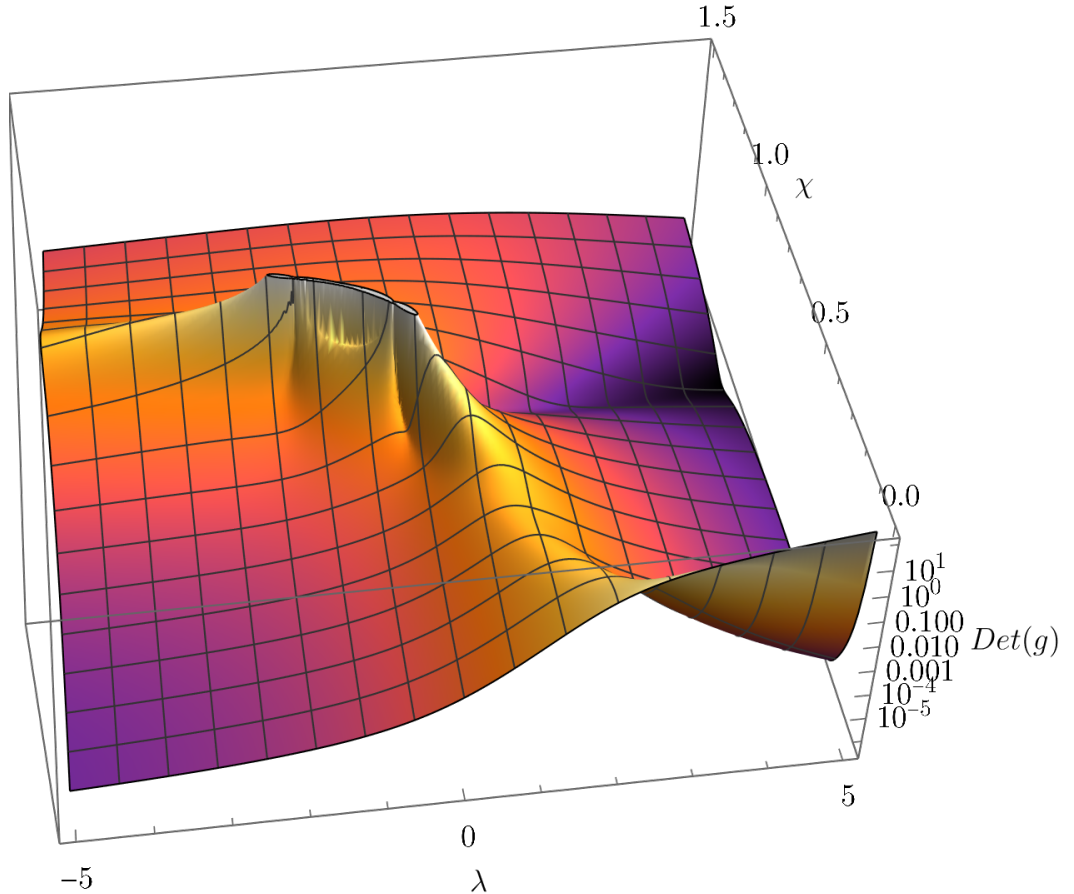


Figure 1.11: Metric tensor determinant for the case $N = 5$.

Geodesics for the case $N = 5$ starting from the point $(0; 0)$ have the characteristics already seen in the case $N = 3$. However, when starting at $(\lambda; \chi) = (1; 0)$, the behavior around the singularity is not the only interesting thing happening. As can be seen in Fig. 1.12, the geodesics tend to deflect themselves from the area with high curvature around the axis $\chi = 0$, which happens even for other initial conditions, just that for $(0; 0)$ it is not so apparent. Small irregularity can be seen in Fig. 1.8 around $(0.5; 0.1)$. This implies that the geodesic equation might have at least two solutions as candidates for the globally shortest path between two points.³ Example of three solutions between two points can be seen in Fig. 1.13.

³The existence of singularities implies that there are infinitely many solutions, because they can bounce between singularities, or go around one of them any number of times. Those are surely not the globally shortest paths, which we are interested in.

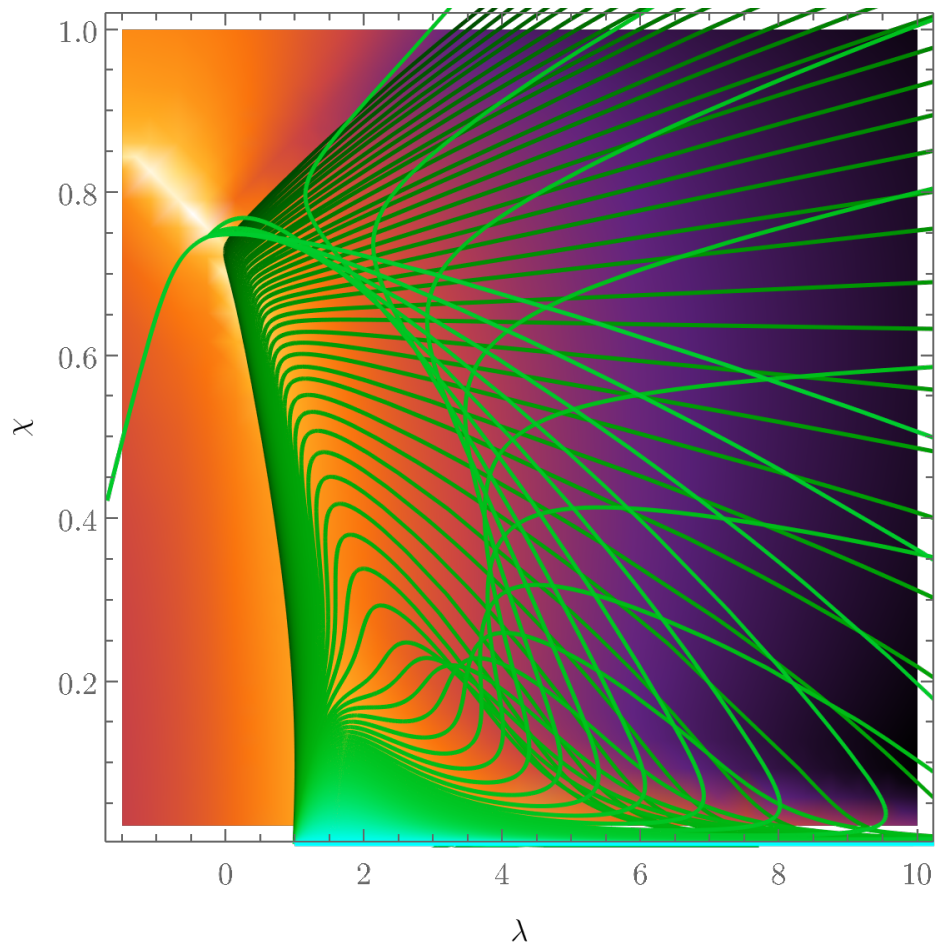


Figure 1.12: Geodesics for the case $N = 5$, starting from the point $(1; 0)$. *The numerics around the singularity breaks down, but the solution is close to the drawn one, i.e. they will pass close to the singularity and continue to the left.*

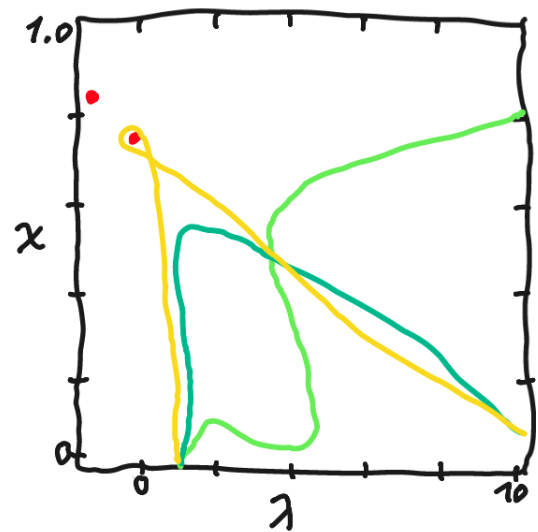


Figure 1.13: Three possible solutions between points $(1; 0)$ and $(4; 0.5)$. The length of the yellow one is surely longer than other two, but the difference between green vs. blue solution is not clear on the first sight.

1.3 Limit $N \rightarrow \infty$

The limit $N \rightarrow \infty$ can be applied to the Hamiltonian in Eq. 1.1 using Holstein-Primakoff mapping for bosonic operators⁴

$$\mathcal{H} := \lim_{j \rightarrow \infty} \frac{\hat{H}}{2j}, \quad (1.15)$$

resulting in classical Hamiltonian

$$\begin{aligned} \mathcal{H}(x, p) = & -\frac{1}{2} + \frac{1-\lambda}{2}x^2 + \frac{\lambda-\chi^2}{4}x^4 - \frac{\chi x^3}{2}\sqrt{2-x^2-p^2} - \frac{\chi^2}{4}p^4 \\ & + \frac{p^2}{4} \left[2 + (\lambda - 2\chi^2)x^2 - 2\chi x\sqrt{2-x^2-p^2} \right]. \end{aligned} \quad (1.16)$$

Finding minimas in its derivatives, we get the *separatrix*

$$\chi^2 = \frac{\lambda - 1}{\lambda - 2}, \quad (1.17)$$

which represents the phase transition in the limit $N \rightarrow \infty$. In our case, the transition is of first order everywhere, except in $(\lambda; \chi) = (1; 0)$, where it has order two. The separatrix is shown in Fig. 1.14 compared to minimum between the ground state and the first excited state $E_1 - E_0$ for $N = 3$ case. With increasing N , it converges to the separatrix line.

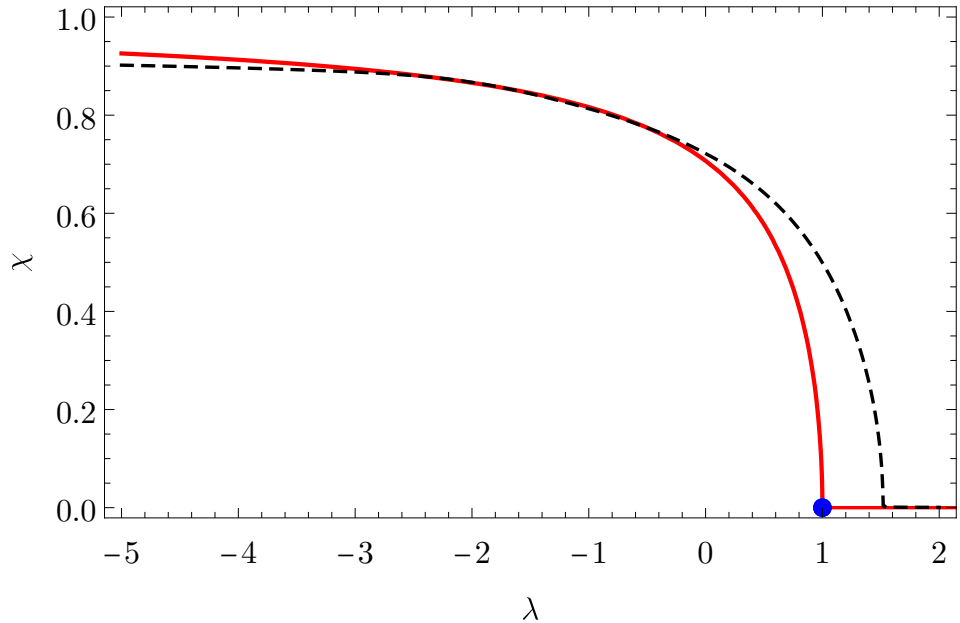


Figure 1.14: First order phase transition – Separatrix (red), second order transition (blue point) compared to minimum between the ground state and first excited state in $N=3$ case (black, dashed).

⁴Felipe did this and I have no idea how

1.4 Arbitrary N

For higher dimensions we see the same characteristic behaviour in the energy spectrum sections, see the example in Fig. 1.15, 1.16 for the $N = 10$ case. Between all energy levels there is at least one avoided crossing and between zeroth and the first there are $N - 2$ crossings for N odd and $N - 3$ for N even, which I have no idea how to prove, but it looks like it might be true.

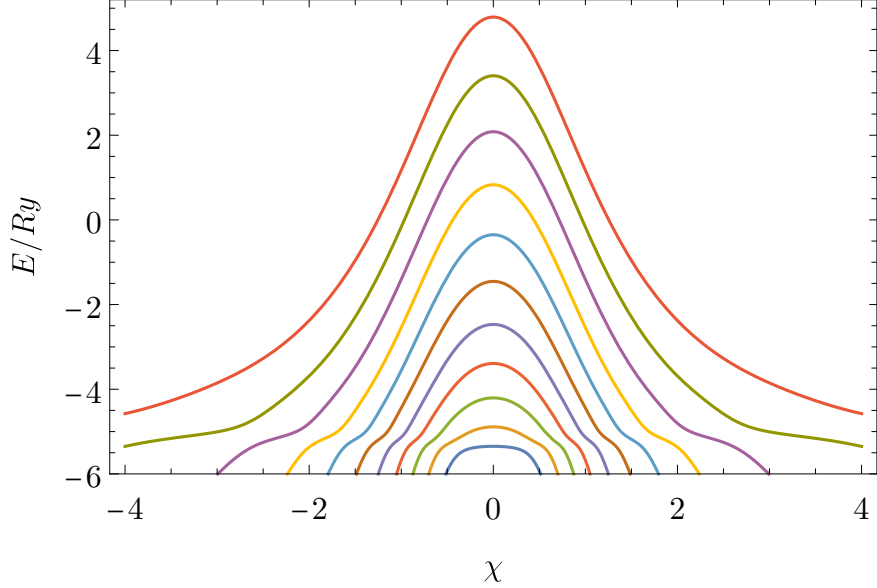


Figure 1.15: Energy spectrum as function of χ , for $\lambda = 1$ and $N = 10$.

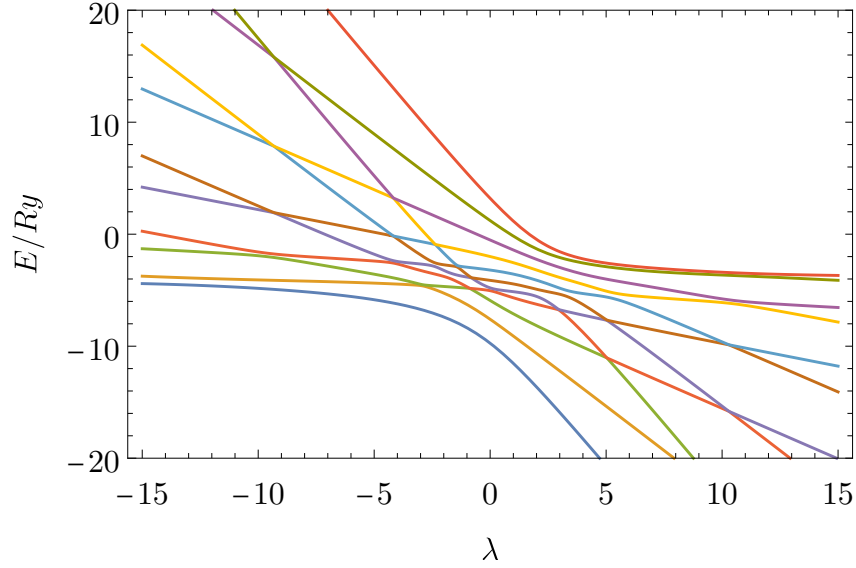


Figure 1.16: Energy spectrum as a function of λ , for $\chi = 1$ and $N = 10$.

Special attention was given to the spectrum degeneracies between the zeroth and the first energy level, because those influence the metric tensor and geodesics. Their exact calculation is numerically costly, and only the first few cases, namely,

$N \in \{3, 4, 5, 6, 7\}$, were calculated, see Tab. 1.1. Those were later proven up to a numerical precision for cases $N \leq 1000$.

N	($\lambda_l; \pm \chi_l$)	($\lambda_2; \pm \chi_2$)	($\lambda_r; \pm \chi_r$)
3	$(-\frac{1}{2}; \sqrt{\frac{3}{5}})$		
4	$(-3; \sqrt{\frac{4}{5}})$		$(-\frac{1}{3}; \sqrt{\frac{4}{7}})$
5	$(-\frac{3}{2}; \sqrt{\frac{5}{7}})$		$(-\frac{1}{4}; \sqrt{\frac{5}{9}})$
6	$(-5; \sqrt{\frac{6}{7}})$	$(-1; \sqrt{\frac{2}{3}})$	$(-\frac{1}{5}; \sqrt{\frac{6}{11}})$
7	$(-\frac{5}{2}; \sqrt{\frac{7}{9}})$	$(-\frac{3}{4}; \sqrt{\frac{7}{11}})$	$(-\frac{1}{6}; \sqrt{\frac{7}{13}})$

Table 1.1: Singularities between the zeroth and first energy levels for dimensions 3–7. Subscript $l(r)$ means the most *left(right)-wise* positioned coordinates in the (λ, χ) -plot.

The observed formula for (λ_l, χ_l) and (λ_r, χ_r) , i.e., those with minimal, resp. maximal λ coordinate is

$$(\lambda_l; \pm \chi_l) = \begin{cases} \left(1 - \frac{N}{2}; \sqrt{\frac{N}{N+2}}\right) & , N \geq 3, N \text{ is odd} \\ \left(1 - N; \sqrt{\frac{N}{N+1}}\right) & , N \geq 3, N \text{ is even} \end{cases} \quad (1.18)$$

$$(\lambda_r; \pm \chi_r) = \left(\frac{1}{1-N}; \sqrt{\frac{N}{2N-1}} \right) \quad , N \geq 3. \quad (1.19)$$

Dimensions 3 to 10 are shown in Fig. 1.17. In addition, the degeneracies between the zeroth and the first energy levels belong to the separatrix described by Eq. 1.17. Due to this, the position of the singularities is constrained to the separatrix between points $(\lambda_l, \pm \chi_l)$ and $(\lambda_r, \pm \chi_r)$.

In the limit $N \rightarrow \infty$ they converge to

$$\lim_{N \rightarrow \infty} (\lambda_l; \pm \chi_l) = (-\infty, 1)$$

$$\lim_{N \rightarrow \infty} (\lambda_r; \pm \chi_r) = \left(0, \frac{1}{\sqrt{2}}\right).$$

One would expect the whole separatrix to be divergent, thus the left limit to be in the $-\infty$, as it is, and the right one to be at the point $(\lambda; \chi) = (1; 0)$, which is not the case. This might mean that some new singularities are being constructed right of λ_r and I will look at it. In addition, because for $N \rightarrow \infty$ there is an infinite number of singularities and because the whole separatrix is divergent, they need to be dense.

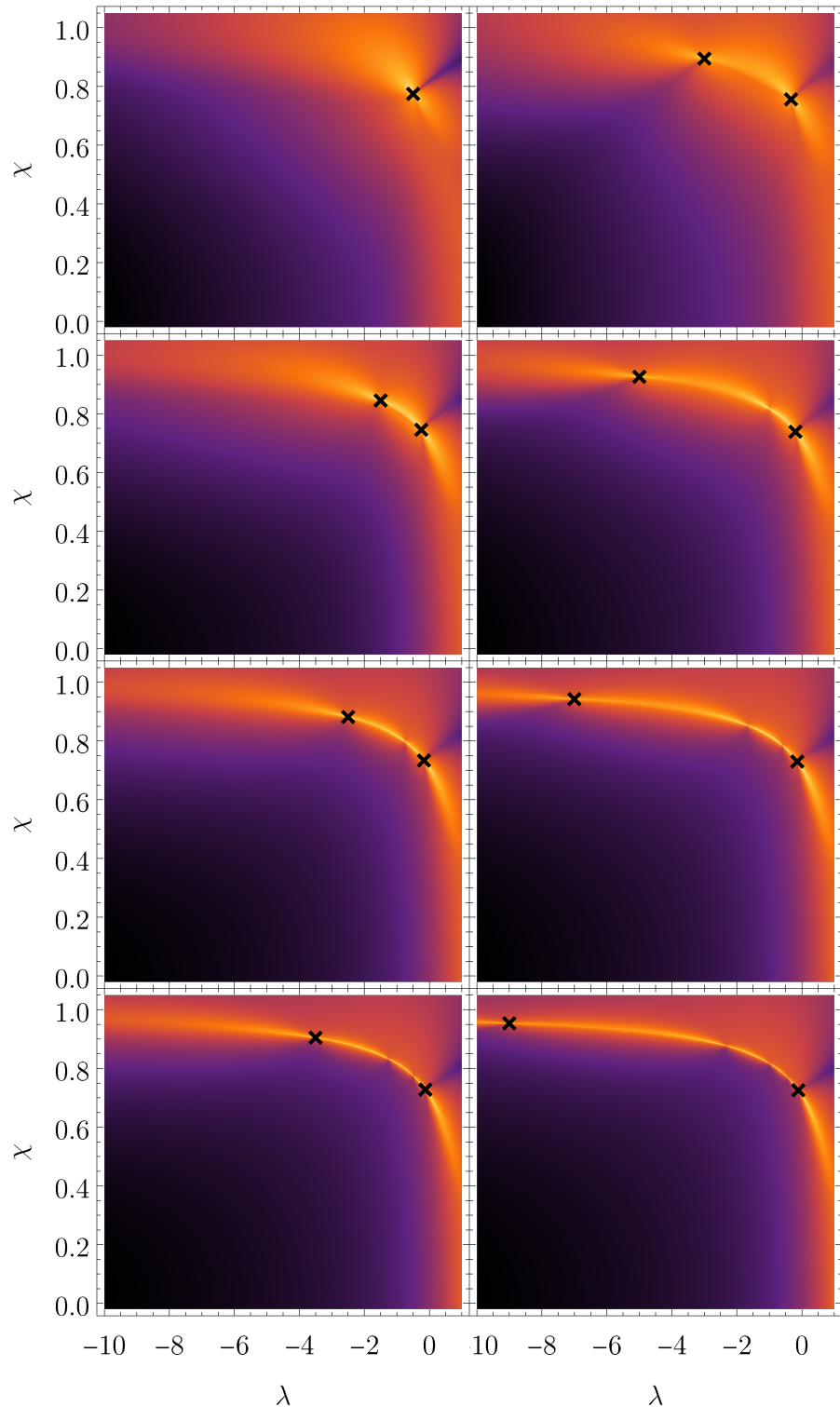


Figure 1.17: Spectrum degeneracy between E_0 and E_1 . Hamiltonian dimensions are 1,3,5,7 in the first column and 2,4,6,8 in the second column. Black crosses mark most left-wise and right-wise singularity and the background corresponds to the metric tensor determinant. Other singularities are also well visible in the determinant.